Lifetimes of flame balls dragged by model turbulent flows: Role of velocity gradient fluctuations

Yves D'Angelo and Guy Joulin*
Laboratoire de Combustion et de Détonique, UPR 9028 du CNRS, ENSMA, 86960 Poitiers, France
(Received 1 October 2003; published 25 March 2004)

An isolated combustion spot—known as a flame ball (FB)—is considered while it is advected by a turbulent flow of a lean premixture of such a light fuel as hydrogen. A Batchelor approximation for the surrounding Lagrangian flow is made. This in principle gives one an access to the FB lifetime t_{life} and to its response to the ambiant Lagrangian rate-of-strain tensor $\mathbf{g}(t)$, by means of a nonlinear and forced integro-differential equation for the current FB radius. For a diagonal $\mathbf{g}(t)$ deduced from random Markov processes of the Ornstein-Uhlenbeck type, or linearly filtered versions thereof, extensive numerical simulations and approximate theoretical analyses agree that (i) flame balls can definitely live for much longer than their time of spontaneous expansion/collapse; (ii) large enough values of t_{life} are compatible with Poisson statistics; (iii) the variations of $\langle t_{life}\rangle$ with the characteristics of $\mathbf{g}(t)$ mirror the latter's statistics, more precisely that of trace($\mathbf{g}^2$). Open problems, dealing with a nondiagonal $\mathbf{g}(t)$, ignition-related transients and/or collective effects, finally are evoked.

DOI: 10.1103/PhysRevE.69.036304 PACS number(s): 47.70.−n, 47.27.−i, 05.45.−a, 02.50.−r

I. INTRODUCTION

For all its practical implications [1–3], the turbulent burning of premixed gases is a central topic in combustion science. Also, its modelling still constitutes a theoretical challenge, because of the many space/time scales and the various nonlinearities (reaction rates, hydrodynamics, radiation) involved.

The current models of turbulent combustion in gases [1] invoke flamelets as building blocks, namely locally laminar flame fronts idealized as surfaces convected by the fresh turbulent medium and propagating relative to it at a normal velocity comparable to the burning speed (S_L) of a steady flat flame. Balancing convection of fresh gas normal to the flamelet with heat conduction (the propagation mechanism) and chemistry classically [2] yields the estimates $D_{th}/t_{ch}(T_b)$ and D_{th}/S_L for S_L and the actual flame thickness, respectively. In these, D_{th} is the fresh gas diffusivity and $t_{ch}(T_b)$ represents the characteristic time of chemical heat release evaluated at the burnt gas temperature T_b in a flat flame.

Whenever the turbulent velocity fluctuations V and the corresponding gradients V/l at scale l of maximum dissipation cease to satisfy $l \gg D_{th}/S_L$ and $V/l \ll 1/t_{ch}(T_b)$, flamelet models cease to be viable, however. Broadened flames, or well-stirred local reactors [1], are usually alluded to when modeling such situations. When the deficient reactant is mobile enough to have a molecular diffusion coefficient D well above D_{th} (Lewis number, $\mathrm{Le} \equiv D_{th}/D \simeq 0.20-0.30$ for hydrogen [H_2] in air), another issue is conceivable. It would involve the localized three-dimensional combustion spots [3] known as flame balls (FB) as building blocks. The basic FB, corresponding to spherically symmetric and convection-free balances between diffusions of heat and reactant and chemical heat release has a reaction temperature T_R of $T_* > T_b$ if $\mathrm{Le} < 1$ [3]. This and the self-explanatory estimate $r_Z^2 \sim D_{th} t_{ch}(T_*)$ for the radius r_Z of this localized combustion spot make it plausible that a FB of $O(r_Z)$ size could resist turbulent stimuli a flamelet would not: $t_{ch}(T_*) \ll t_{ch}(T_b)$ if, as is usual, the Zel'dovich number $\mathrm{Ze} \sim -\partial \log t_{ch}/\partial \log T_R$ is large whence $t_{ch}(T_R)$ is strongly sensitive to the reaction temperature T_R. Hence the notion of envisaging FBs as basic ''objects'' dragged by the flow for the premixed combustion of light fuels under conditions of vigorous turbulent stirring.

The basic (i.e., adiabatic and convection-free) FB is unstable, however [3,4]: it spontaneously tends to shrink then extinguish, or to expand radially and evolve into a thin propagating front [5]. Stabilizing processes have been identified and can preclude such trends [6,7]. They share a common structural property: they all make T_R slightly decrease, with a $\delta T_R \equiv T_R - T_* < 0$ and at least linear in the current FB radius $r_F(t)$. The net result is that r_F may ultimately settle at a larger value than r_Z. For very lean/diluted H_2-air premixtures, the radiation losses do the job, enabling FB's to be observed up to 80 minutes at microgravity [8]. With less diluted and/or with preheated mixtures, the radiative cooling time would be too long compared to $t_{ch}(T_*)$ to achieve FB stabilization. Whence apparently little hope is left for FBs to be thought of as sensible starting points to model the strongly turbulent combustion of light fuels.

Yet a localized combustion spot of $O(r_Z)$ size advected by a turbulent flow, Fig. 1, also feels the $O(V/l)$ velocity gradients in the surrounding fresh mixture; because heat and reactant transports respond differently to nonuniform/unsteady flowfield if $\mathrm{Le} < 1$, this affects δT_R hence the FB dynamics. As shown in [5], the order-of-magnitude estimate $\delta T_R/T_* \sim (D^{-1/2} - D_{th}^{-1/2})(V/l)^{1/2} r_F < 0$ holds true if $l \gg r_F$. Thus, the interesting distinguished limit to consider has $V/l \sim \mathrm{Ze}^{-2} D_{th} r_Z^{-2}$, because this yields $\delta T_R/T_* \sim \mathrm{Ze}^{-1}$ and hence fully exploits the nonlinearity of the $t_{ch}(T_R)$ law. Also, having $\delta T_R < 0$ and linear in r_F almost brings one back to a familiar situation.

*Electronic address: dangelo@lcd.ensma.fr

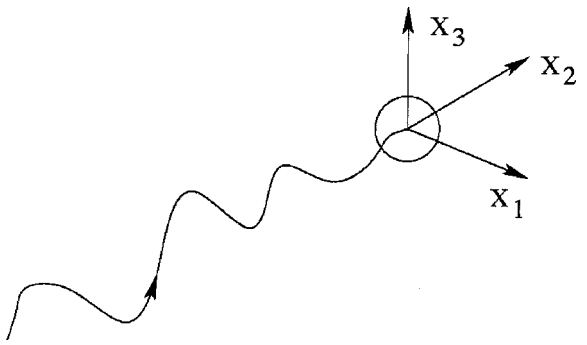

FIG. 1. An isolated flame ball advected by a turbulent flow.

The above estimates imply that the spatial scale $V/(V/l) \sim l$, where flowfield nonuniformity effectively plays a role, is large [of order $O(\mathrm{Ze}\, r_F)$] compared to the FB size. This scale separation enabled one [5] to show that not-too-intense combinations of *steady* shears, strains, and flow rotations can effectively stabilize a FB at $r_F/r_Z = O(1)$. Thanks to the fact that the time of spontaneous evolution of r_F about r_Z is $O(\mathrm{Ze}^2 r_F^2/D_{th}) \gg r_F^2/D_{th}$ [9], implying quasisteady evolutions of the FB core, the conclusion was recently extended to FB's embedded in periodic or quasiperiodic uniform shearing or straining motions of $O(D_{th}/\mathrm{Ze}^2 r_Z^2)$ strengths: the integro-differential, nonlinear evolution equation (EE) derived for r_F in [10] then allowed for limit cycles (or kins) as attractors corresponding to infinitely long-lived flame balls, as first evidenced numerically and by formal asymptotics [10], then rigorously proved [11].

To get closer to the physical situation depicted in Fig. 1, we consider here the dynamics of an isolated FB subjected to random, yet again spatially uniform like in [10], velocity gradients. The motivation is as follows: occasionally large values of the rate-of-strain tensor that a FB embedded in a turbulent flow experiences can possibly *always* lead to extinguishment, contrary to bounded periodic/quasiperiodic stimuli.

Since the EE recently established for r_F [10] involves memory kernels, the very possibility of a fluctuation-induced limitation of FB lifetimes raises the question: how to initiate the dynamics. This "past-boundary-difficulty" could be eliminated upon explicitly accounting for an ignition device (or a mathematical analog thereof in the EE). Unfortunately, the resulting dynamics is not easily interpreted if no information about the intrinsic role of velocity fluctuations is available beforehand. To display the latter in an as pure as possible way, we shall here content ourselves with studying a switch-on problem: the velocity-gradient fluctuations are artificially suppressed for all negative times then restored at $t=0$ and allowed to influence the subsequent dynamics. The EE for $r_F(t)$, once properly discretized and solved, gives numerical access to the individual FB histories, then to their statistics.

The paper is organized as follows. The physical model for a flame ball is presented in Sec. II, along with a sketch of the derivation that leads to an evolution equation (EE) for the FB radius. Section III is devoted to the generation of random velocity gradients and to the switch-on procedure. The numerical method to solve the EE is summarized in Sec. IV. In Sec. V, we report on raw numerical findings: memory kernels, heat-loss functions, FB trajectories and lifetimes, and statistics thereof; these are compared to tentative theoretical interpretations in Sec. VI. Section VI C aims at extending all this to non-Gaussian velocity gradients. We end up with conclusions and open problems.

II. MODEL AND EVOLUTION EQUATION

Like in [10], we envisage a turbulent premixture of a deficient mobile fuel (e.g., H_2) and of an abundant oxidizer (e.g., air), and focus attention on an isolated flame ball dragged [23,24] by the turbulent motions (see Fig. 1).

The selected combustion process is the one-step irreversible reaction "$F \rightarrow$ products + heat," where F stands for the fuel. Its volumetric rate of consumption w will follow the Arrhenius law:

$$w(T,y) = \rho y \exp(-T_a/T)/t_{\mathrm{coll}} \tag{1}$$

that involves a collision time t_{coll} and an activation temperature T_a large compared to all the temperatures T encountered. The mixture density is denoted ρ and is assumed to vary like $1/T$. The fuel mass fraction is y.

The mass and energy conservations and the fuel balance are respectively written as

$$\partial_t \rho + \boldsymbol{\nabla} \cdot (\rho \mathbf{v}) = 0, \tag{2}$$

$$\rho c (\partial_t T + \mathbf{v} \cdot \boldsymbol{\nabla} T) = \lambda \boldsymbol{\nabla}^2 T + Q w(T,y), \tag{3}$$

$$\rho (\partial_t y + \mathbf{v} \cdot \boldsymbol{\nabla} y) = \rho D \boldsymbol{\nabla}^2 y - w(T,y), \tag{4}$$

In Eqs. (2)–(4), Q is the heat of reaction, $\partial_t(\cdot)$ denotes differentiation in time t and $\mathbf{v}$ is the local velocity vector in the Cartesian frame $\mathbf{x} = (x_1, x_2, x_3)$ attached to the flame ball center $r \equiv |\mathbf{x}| = 0$. We consider the specific heat c, the heat conductivity λ and the product ρD of density by the fuel diffusivity D as prescribed constants. The Lewis number $\mathrm{Le} = D_{th}/D = \lambda/\rho D c$ is thus constant and assumed to be markedly less than one (e.g., $\mathrm{Le}_{\mathrm{H_2\text{-}air}} \simeq 0.20-0.3$). Far from the flame ball, we require

$$y(+\infty, t) = y_u, \tag{5}$$

$$T(+\infty, t) = T_u, \tag{6}$$

$$\mathbf{v}('\infty', t) \rightarrow \mathbf{g}(t) \cdot \mathbf{x} \equiv \mathbf{v}_\infty, \tag{7}$$

where y_u and T_u are given, and "∞" in Eq. (7) means "for $r \gg r_F(t)$," r_F being the current flame ball radius.

The rate of strain tensor $\mathbf{g}$, of elements $g_{ij}(t)$, satisfies the incompressibility condition

$$\mathrm{trace}(\mathbf{g}) \equiv \boldsymbol{\nabla} \cdot \mathbf{v}_\infty = 0 \tag{8}$$

for the sake of compatibility with Eqs. (7) and (2), and is assumed to vanish on time average:

$$\overline{g_{ij}(t)} = 0. \tag{9}$$

The present work next considers the g_{ij}'s to be *random* functions of time, with a common autocorrelation time t_{cor} and identical PDFs.

In absence of any flow ($\mathbf{v}=\mathbf{0}$) and for steady configurations, Eqs. (2)–(7) admit the first-integral $\lambda T+\rho D y Q \equiv \lambda T_u+\rho D y_u Q$. Setting y to zero in it defines the reference reaction temperature $T_*=T_u+(T_b-T_u)/\mathrm{Le}$ where $T_b=T_u+Qy_u/c$ is the final temperature in a flat flame propagating in a fresh mixture that has $y=y_u$, $T=T_u$. In the limit $\mathrm{Ze}\equiv T_a(T_b-T_u)/T_*^2\to+\infty$ of large Zel'dovich numbers we again adopt here, the steady convection-free flame ball has chemical activity confined to a thin spherical shell $r-r_Z=O(r_Z/\mathrm{Ze})$ with (see [5,10] and the references therein)

$$2r_F^2=D(T_R)t_{\mathrm{coll}}\left(\frac{T_a(T_b-T_u)}{T_R^2}\right)^2\exp\left(\frac{T_a}{T_R}\right) \tag{10}$$

and, here, $T_R=T_*$ and hence $r_F=r_Z$. Such a flame ball is unstable [4] and the typical time t_Z for spontaneous evolutions of r_F-r_Z is $t_Z=\mathrm{Ze}^2r_Z^2/D_{th}$ if $0<1-\mathrm{Le}=O(1)$ and $\mathrm{Ze}\gg 1$ [9], hence is long compared to the conduction time r_Z^2/D_{th}. Insofar as their reaction-shell radius $r_F(t)$ remains $O(r_Z)$, flame balls evolving over $O(t_Z)$ time scale have a quasi steady near-field $r=O(r_F)$, where unsteadiness and convection may be neglected [5,10]; the convection due to $\partial_t r_F\neq 0$ may also be neglected in the far field $r=O(\mathrm{Ze}\, r_F)$ where $T\simeq T_u$ and $y\simeq y_u$ and unsteadiness [and imposed convection if $g(t)\neq\mathbf{0}$] plays a role. Matching the near-field and far-field profiles of T and y reveals that Eq. (10) still holds for the current $r_F(t)$, provided T_R is shifted from T_* to $T_*+\delta T_R$, with

$$\delta T_R=\delta T_\infty+(T_*-T_u)\,\delta y_\infty/y_u\,. \tag{11}$$

In Eq. (11), δT_∞ and δy_∞ are displacements, induced by unsteadiness and/or forced convection in the far field, of the ambient temperature and fuel mass fraction actually felt by the flame ball core. The corresponding $r_F(t)$, given by Eq. (10) if $\delta T_R/T_*=O(\mathrm{Ze}^{-1})$, reads

$$(r_F/r_Z)^2=\exp\left(-\frac{\delta T_R}{T_*}\frac{T_a}{T_*}\right) \tag{12}$$

to leading order. Provided the velocity gradients $g_{ij}(t)$ featured in Eq. (7) are $O(t_Z^{-1})$ and evolve on the $t_{cor}=O(t_Z)$ scale, Eq. (12) holds and the fact that $\mathbf{g}$ is not identically zero contributes to δT_R at the same order as unsteadiness. As first shown in [12] the then linear [$\rho\simeq\rho_u$, negligible $w(T,y)$] Eqs. (3) and (4) can be solved analytically in the far-field when Eq. (7) holds, with the leading order matching conditions: $(T-T_u)r\to(T_*-T_u)r_F$ and $(y-y_u)r\to -y_u r_F$ as $r/\mathrm{Ze}\to 0^+$. Through two-term matchings, this altogether yields [10]

$$\frac{(4\pi D_{\mathrm{th}})^{1/2}\delta T_\infty}{T_*-T_u}=-\int_{-\infty}^{t}ds\left[\frac{r_F(t)}{(t-s)^{3/2}}-\frac{r_F(s)}{\aleph^{1/2}(t,s)}\right], \tag{13}$$

$$\frac{(4\pi D)^{1/2}\delta y_\infty}{y_u}=+\int_{-\infty}^{t}ds\left[\frac{r_F(t)}{(t-s)^{3/2}}-\frac{r_F(s)}{\aleph^{1/2}(t,s)}\right], \tag{14}$$

where $\aleph(t,s)$ is the determinant of an auxiliary symmetric tensor $\mathbf{b}(t,s)$, defined by the coupled ODE's (with the usual convention on repeated indices)

$$\partial_t b_{ij}=\delta_{ij}+g_{il}b_{lj}+b_{il}g_{jl}\quad\text{for } t\geqslant s,$$

$$b_{ij}(t,s)=(t-s)\,\delta_{ij}+\cdots\quad\text{for } t=s+0. \tag{15}$$

Note that $b_{ij}\equiv(t-s)\,\delta_{ij}$ and $\aleph(t,s)\equiv(t-s)^3$ for $g_{ij}\equiv 0$; this also holds true if $g_{ij}=-g_{ji}$. Substitution of Eqs. (13) and (14) into Eq. (11) then Eq. (12) yields [10] the evolution equation for $r_F(t)$:

$$\log\left(\frac{r_F(t)}{r_Z}\right)=\mathrm{Ze}\frac{1-\sqrt{\mathrm{Le}}}{2\mathrm{Le}}\frac{1}{(4\pi D_{th})^{1/2}}\times\int_{-\infty}^{t}\left[\frac{r_F(t)}{(t-s)^{3/2}}-\frac{r_F(s)}{\aleph^{1/2}(t,s)}\right]ds \tag{16}$$

in which the nonzero tensor $\mathbf{g}$ intervenes *via* the solution $\mathbf{b}(t,s)$ to system (15). Notice that despite the formal symmetry between Eqs. (13) and (14), and Eq. (11), δT_R does not vanish when $0<1-\mathrm{Le}=O(1)$, so that r_F may differ from r_Z without violating the working assumptions employed to derive Eq. (16).

In the general case $\mathbf{g}$ is nonsymmetric. Its skew-symmetric part is known [10,12] to make the influence of the straining parts milder on such displacements as δT_∞, δy_∞ and δT_R. The effects are thus maximum when $g_{ij}=g_{ji}$. For analytical convenience, we further restrict ourselves to $\mathbf{g}=\mathrm{diag}(g_1(t),g_2(t),g_3(t))$, with $g_1+g_2+g_3=0$ by Eq. (8), corresponding to pure straining motions. Equation (15) can then be formally solved for $\mathbf{b}(t,s)$—which is also diagonal in this case—by quadratures.

III. NOISES

A. Random rates of strain

The strain rates are written in the form

$$g_i(t)=\frac{\mu}{t_{cor}}\Gamma_i\left(\frac{t}{t_{cor}}\right), \tag{17}$$

where $t_{cor}\geqslant O(t_Z)$ is their common correlation time. The Γ_i's are $O(1)$ and dimensionless, μ is a pure number, measuring the intensity of the g_i's in $1/t_{cor}$ units. For a solid-body rotation, $|\mu|=2\pi$. For the sake of definiteness, $\mu>0$ is assumed. Setting $t/t_{cor}=u$, the Γ_i's are computed as

$$\Gamma_i=H_i-\frac{1}{3}(H_1+H_2+H_3) \tag{18}$$

from three independent Ornstein-Uhlenbeck [13,22] stochastic processes $H_i(u)$ [25]; the latter are numerically generated by means of the recursions

$$\frac{H_i(u_{n+1})-H_i(u_n)}{\delta u}=-\frac{H_i(u_n)}{1}+\varepsilon_i^n\kappa(\delta u) \tag{19}$$

where δu is the scaled time step, $u_n=n\,\delta u$, $\kappa(\delta u)\equiv(3/\delta u\times(2-\delta u))^{1/2}$ and the ε_i^n are random numbers sampled uniformly over $[-1;+1]$, independently of n and i; for $u_n\leqslant u\leqslant u_{n+1}$, the $H_i(u)$ are assumed piecewise linear, and are continuous at the mesh points u_j.

For $n\,\delta u\gg 1$, the H_i are Gaussianly distributed [26,13], have unit variance, zero time and ensemble averages, and their autocorrelation function is $\exp(-|u|)$ [and hence their temporal spectral density is $\sim(1+\omega^2)^{-1}$]. By Eq. (18), the Γ_i's sum to zero, are Gaussian with a common rms value of $(2/3)^{1/2}$, and are also exponentially autocorrelated.

B. Nondimensional evolution equation

Setting $r_F=r_Z\mathcal{R}(u)$ and using u as dimensionless time variable converts Eq. (16)—after some rearrangements—into

$$\int_{-\infty}^{u}\frac{\mathcal{R}(u)-\mathcal{R}(v)}{\Delta^{1/2}(u,v)}dv=\sqrt{\tau}\log\mathcal{R}-A(u)\mathcal{R}, \tag{20}$$

in which *all* the relevant physico-chemical properties of the gaseous mixture are lumped into the single parameter τ

$$\tau=4\pi\frac{t_{cor}}{t_Z}\left(\frac{2\mathrm{Le}}{1-\sqrt{\mathrm{Le}}}\right)^2,\quad t_Z\equiv \mathrm{Ze}^2r_Z^2/D_{th}. \tag{21}$$

This grouping essentially measures t_{cor} in units of $t_Z/4\pi$, since $2\mathrm{Le}=1-\sqrt{\mathrm{Le}}$ for $\mathrm{Le}=0.25$. Should the quasisteady limit $\tau\gg 1$ be considered later on, the limit $\mu\gg 1$ would also be needed, as the velocity gradients would otherwise cease to influence the FB dynamics [see Eq. (17)] for $\mathcal{R}\leqslant O(1)$. The symbol $\Delta(u,v)$ is a scaled version of the determinant $\aleph(t,s)$ of the **b** tensor featured in Eqs. (13)–(16); in the present case, it can be explicitly derived as

$$\Delta(u,v)=\prod_{i=1}^{3}\int_v^u\exp\left(-2\mu\int_u^w\Gamma_i(\xi)d\xi\right)dw \tag{22}$$

once the incompressibility condition $\Sigma_{i=1}^3\Gamma_i=0$ is made use of. As shown in [10], $\Delta(u,v)$ is strictly larger than $(u-v)^3$ for $u>v$, whenever all the Γ_i's are not identically zero. The scaled heat-loss function $A(u)>0$, appearing in Eq. (20), is defined by

$$A(u)=\int_{-\infty}^{u}\left(\frac{1}{(u-v)^{3/2}}-\frac{1}{\Delta^{1/2}(u,v)}\right)dv. \tag{23}$$

It would assume the constant value $A(0)=\sqrt{\mu}I$, with

$$I\equiv\int_0^{+\infty}\left(1-\prod_{i=1}^{3}F(\Gamma_i(0)w)\right)w^{-3/2}dw, \tag{24}$$

$$F(Z)=(Z/\sinh Z)^{1/2}, \tag{25}$$

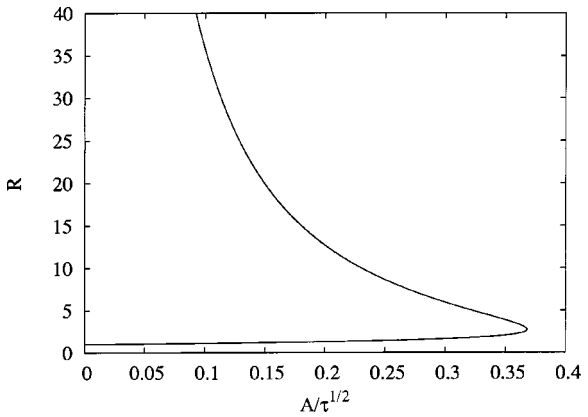

FIG. 2. Static response curve: the equation $A(0)/\sqrt{\tau}=\log R/R$ admits two solutions if $A(0)<\sqrt{\tau}\exp(-1)$. Too strong constant strain rates quench a flame ball, if $A^2(0)/\tau>e^{-2}$.

if the Γ_i's were constants $[\equiv\Gamma_i(0)]$. Equation (20) would then admit constant solutions R's $[=R(0)]$ given by the roots $R_\pm$ (with $1\leqslant R_-\leqslant e$ and $R_+\geqslant e$) of the equation

$$\frac{A(0)}{\sqrt{\tau}}=\frac{\log R}{R}, \tag{26}$$

that exist if and only if $A(0)\leqslant\sqrt{\tau}\exp(-1)$; see Fig. 2: too strong, steady strain rates will quench a flame ball, e.g., if μ is too large [indeed, $A^2(0)/\tau\sim(\mu/\tau)$ then simply measures the intensity of the $g_i(0)$'s; see Eq. (17)]. For future reference notice that—as first suggested in [12]—the integral $I(\Gamma_1(0),\Gamma_2(0),\Gamma_3(0))$ featured in the RHS of Eq. (24) is close to a function of the "total strain"

$$\Gamma\equiv[\Gamma_1^2+\Gamma_2^2+\Gamma_3^2]^{1/2} \tag{27}$$

only, here evaluated at $u=0$. We numerically ascertained that, when $\Gamma_1+\Gamma_2+\Gamma_3=0$ as required by Eq. (8), the integral I is almost undistinguishable from the formula

$$I^2(\Gamma_1,\ \Gamma_2,\ \Gamma_3)\simeq\sqrt{\frac{8}{3}}\Gamma, \tag{28}$$

that actually is exact when the $|\Gamma_i|$'s are in the ratios 1:1/2:1/2 [since $I(1,1/2,1/2)=\sqrt{2}$].

IV. NUMERICS, PAST BOUNDARY DIFFICULTY

A. Fluctuation switch-on

Whereas the lower bound $v=-\infty$ in the LHS of Eq. (20) poses no convergence problem $[\Delta(u,v)>(u-v)^3]$, the use of *random* Gaussian H_i's implies that one of them may occasionally take on a large absolute value, at which times the Γ_i's may also get large for long enough to extinguish the flame ball. The net result is that $\mathcal{R}(u)$ cannot live for infinitely long and, in particular, cannot have lived since $u=-\infty$.

To cure this past-boundary difficulty, that in a sense is analogous to the cold-boundary difficulty in the theory of steady planar premixed flames [1], the following procedure

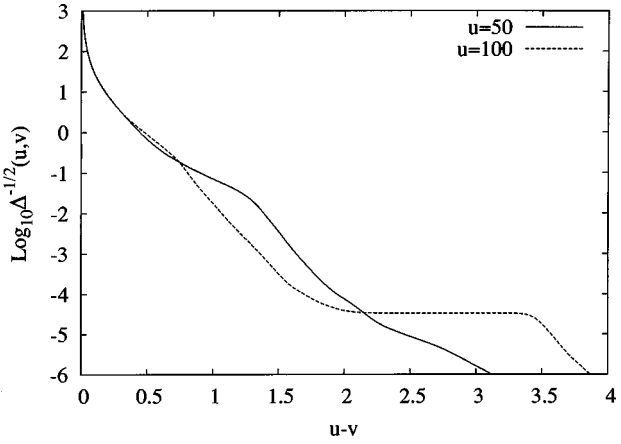

FIG. 3. Sample memory kernels $\Delta^{-1/2}(u,v)$ for two values of current time u, and $\mu=5$. The fast decrease with increasing $u-v$ is worth noticing.

of fluctuation switch-on was devised. For a given sample triplet $[\Gamma_1(u), \Gamma_2(u), \Gamma_3(u)]$, we made the substitution $\Gamma_i(u)\to\tilde{\Gamma}_i(u)$ with

$$\tilde{\Gamma}_i(u)=\Gamma_i(0) \text{ for } u\leqslant 0, \quad \tilde{\Gamma}_i(u)=\Gamma_i(u) \text{ for } u\geqslant 0, \tag{29}$$

along with the corresponding changes in Eqs. (22) and (23). In particular, the modified heat-loss function $\tilde{A}(u\leqslant 0)$ is equal to $A(0)$ for negative times, as it is given by Eq. (24). For negative times, the dimensionless flame ball radius $\mathcal{R}(u\leqslant 0)$ was chosen to be the larger (hence stable [11]) root R_+ of Eq. (26), if any. Whenever $A(0)>\sqrt{\tau}\exp(-1)$, a new triplet of $\Gamma_i(u)$'s was sampled afresh. This ''fluctuation switch-on'' procedure is analogous to rendering the chemical time infinite below an ignition temperature (assumed to be crossed at the coordinate origin) in premixed-flame theory [1].

Because $\Delta^{-1/2}(u,v)$ decreases rapidly as $u-v$ increases (see Fig. 3), implying rapidly fading memory effects, the transient resulting from the reintroduction of fluctuations is expected to be short $[0<u\leqslant O(\mu^{-1})]$ and negligible at the scale of the flame ball lifetime u_{life}, especially if $u_{life}\gg 1$.

B. Random processes

Handling the recursion (19) poses no particular problem, provided one makes sure it has started long enough before $u=0$, so that the H_i's have already forgotten the initial conditions. Our numerical simulations employed 10^4 ''blank'' steps, with a δu of 10^{-2}. As the latter is meant to be smaller than all the relevant time scales of the problem, in particular $(u-v)=O(1/\mu)$ (see Sec. VI), μ's larger than 10 could not be handled at reasonable CPU cost *and* in a reliable way.

C. Kernel storage

Even though an explicit expression for $\Delta(u,v)$ is available, Eq. (22), better numerical accuracy and stability were at first found upon directly integrating the differential system (15). However, if this procedure were applied abruptly, the calculation of $\Delta(u,v)$ for long times u and v would require to store a two-variable array with several tens of thousand elements in both time variables, for each realization of the H_i's, before any attempt at solving Eq. (20). This storage difficulty can be circumvented once one has noticed that $\Delta(u,v)$ in Eq. (22) can be written as $\Delta(u,v)=\Pi_{i=1}^{3}\Delta_i(u,v)$, and that the $\Delta_i(u,v)$ are also accessible from the differential system

$$\frac{\partial\Delta_i}{\partial v}=-\varpi_i^2(u,v), \quad \Delta_i=0 \text{ at } v=u, \tag{30}$$

$$\frac{\partial\varpi_i}{\partial v}=-\mu\tilde{\Gamma}_i(v)\varpi_i(u,v), \quad \varpi_i=1 \text{ at } v=u. \tag{31}$$

In these ODEs, integration is performed with respect to $v\leqslant u$, *at fixed u*, whereby no two-variable array at all needs be stored prior to the resolution of Eq. (20).

D. Integrating the evolution equation

To integrate the evolution equation (20) for the dimensionless FB radius $\mathcal{R}$, we proceed as follows. The differential system (30) and (31) is advanced in time thanks to a multistep, variable-coefficient, stiff ODE solver [14]. The left-hand side of Eq. (20) is split into two integrals, for negative and positive v respectively; for negative v, $\mathcal{R}(v)\equiv R_+$ [see Eq. (26)]. These two terms can then be processed as

$$\begin{aligned}\int_{-\infty}^{u}\frac{\mathcal{R}(u)-\mathcal{R}(v)}{\Delta^{1/2}(u,v)}dv &= (\mathcal{R}(u)-R_+)\int_{-\infty}^{0}\Delta^{-1/2}(u,v)dv \\ &+\mathcal{R}(u)\int_{0}^{u-\delta u}\Delta^{-1/2}(u,v)dv \\ &-\int_{0}^{u-\delta u}\frac{\mathcal{R}(v)}{\Delta^{1/2}(u,v)}dv+\int_{u-\delta u}^{u}\frac{\mathcal{R}(u)-\mathcal{R}(v)}{\Delta^{1/2}(u,v)}dv.\end{aligned} \tag{32}$$

For numerical consistency, the integration is first performed from $-\infty$ to $u-\delta u$ where δu is the time step size. The last integral in Eq. (32) can be evaluated as

$$\int_{u-\delta u}^{u}\frac{\mathcal{R}(u)-\mathcal{R}(v)}{\Delta^{1/2}(u,v)}dv\simeq 2(\mathcal{R}(u)-\mathcal{R}(u-\delta u))/\sqrt{\delta u}. \tag{33}$$

The scaled heat-loss function $A(u)$ defined by Eq. (23) can also be split into parts:

$$\begin{aligned}A(u)=&\int_{-\infty}^{0}\frac{1}{(u-v)^{3/2}}dv-\int_{-\infty}^{0}\frac{1}{\Delta^{1/2}(u,v)}dv \\ &+\int_{0}^{u}\left(\frac{1}{(u-v)^{3/2}}-\frac{1}{\Delta^{1/2}(u,v)}\right)dv.\end{aligned} \tag{34}$$

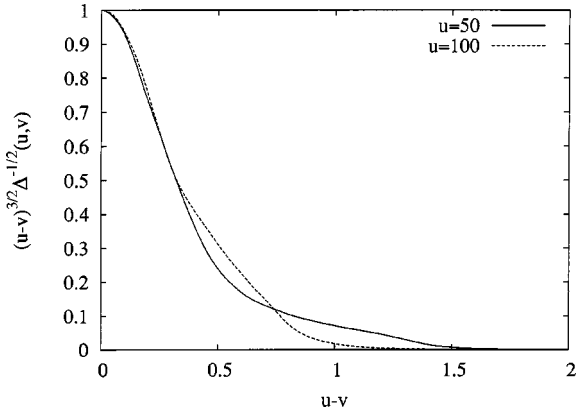

FIG. 4. Sample reduced memory kernels $\mathcal{K}(u,v)\equiv(u-v)^{3/2}/\Delta^{1/2}$ for two values of current time u (same runs as in Fig. 3).

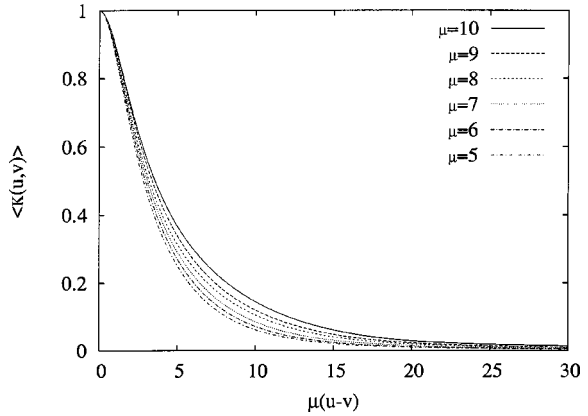

FIG. 5. Ensemble average of the reduced memory kernel $\mathcal{K}(u,v)$ vs $u-v$, for different values of μ.

The first term of the right-hand side of Eq. (34) equals $2/\sqrt{u}$. The second term already appeared in Eq. (32). For a given discretization time u_{n+1}, we approximate the third integral in the right-hand side (RHS) of Eq. (32) assuming $\mathcal{R}(v)$ to be piecewise linear (between u_k and u_{k+1}). The integrals involving $\Delta^{-1/2}(u_{n+1},v)$ are also computed by means of the trapezoidal rule [i.e., assuming $\Delta^{-1/2}(u_{n+1},v)$ piecewise linear between v_k and v_{k+1}]. Last, the evolution equation is discretized semi-implicitly in time: the linear terms are treated implicitly [i.e., with $\mathcal{R}(u)$ evaluated at time u_{n+1}] whereas the nonlinear terms are treated explicitly [i.e., with $\mathcal{R}(u)$ evaluated at time u_n]. At anyone time step, this procedure leads to a linear equation for $\mathcal{R}_{n+1}$, the coefficients of which depend on the whole past history of $\mathcal{R}$. Notice that the integrals in v involving the kernel $\Delta^{-1/2}(u_{n+1},v)$ need be reevaluated at each new meshpoint, since the kernel explicitly depends on the current u_{n+1}.

When $u-v$ equals one or a few time step(s) δu, evaluating the integrals as above is not accurate enough. We then had to subcycle the time stepping procedure with a smaller step size δu_{sc}, equal to a fraction (1/10 or 1/20) of δu.

E. Benchmark

In order to validate the whole numerical procedure, we applied it to a benchmark where an analytical solution can be found for $A(u)$ if $\mathcal{R}(u)$ and the kernel are given *a priori*. Namely, we choose to solve the equation

$$\int_{-\infty}^{u}(\mathcal{R}(u)-\mathcal{R}(v))W(u-v)dv=\sqrt{\tau}\log\mathcal{R}-A(u)\mathcal{R}, \tag{35}$$

with $\mathcal{R}(u)=R_+-1+\cos(u)$. If $W(u-v)\equiv(u-v)^{-3/2}$, the expression for $A(u)$ then involves (tabulated) sine and cosine Fresnel integrals. Retrieving the known $\mathcal{R}(u)$ from that $A(u)$ was the test successfully passed by the procedure (30)–(32).

V. RAW RESULTS

A. Memory kernels and heat-loss functions

Figure 4 illustrates how the reduced memory kernel $(u-v)^{3/2}/\Delta^{1/2}\equiv\mathcal{K}(u,v)$ varies with $v\leqslant u$ at different fixed positive u, making it clear that the memory kernel involved in the LHS of Eq. (20) fades much more quickly than in absence of velocity gradients [$\mathcal{K}(u,v)\equiv 1$ for $\mu\Gamma_i\equiv 0$], especially when $|\mu|$ is large; the latter trend, meaning that random incompressible straining flows of increasing intensities have better and better mixing properties, is illustrated in Fig. 5, in terms of the ensemble average $\langle\mathcal{K}(u,v)\rangle$ of the memory kernel for different values of μ. Notice that $\mathcal{K}(u,v)\to 1^-$ as $v\to u^-$. Indeed, one can show from Eq. (22) or Eqs. (30) and (31) that $1-\mathcal{K}(u,v)\sim\mu^2(u-v)^2\Sigma_{i=1}^3\Gamma_i^2(u)$ in this limit, which suggested to us that $u-v=O(1/\mu)$ is the right range of memory effects for large enough μ's. As compared to the spontaneous dynamics [9], wherein a 1/2-order derivative was involved [$\Delta^{1/2}(u,v)=(u-v)^{3/2}$ then], the linear operator in the LHS of Eq. (20) is here closer to a "thickened" first-order derivative [see Eq. (A1) of Appendix A].

A sample heat-loss function [27] $A(u)$ is displayed in Fig. 6 and compared to one of the Γ_i's that yielded it: due to the integration steps involved in Eqs. (30) and (31) then Eq. (23), $A(u)$ is smoother than the Γ_i's. Whereas the H_i's have

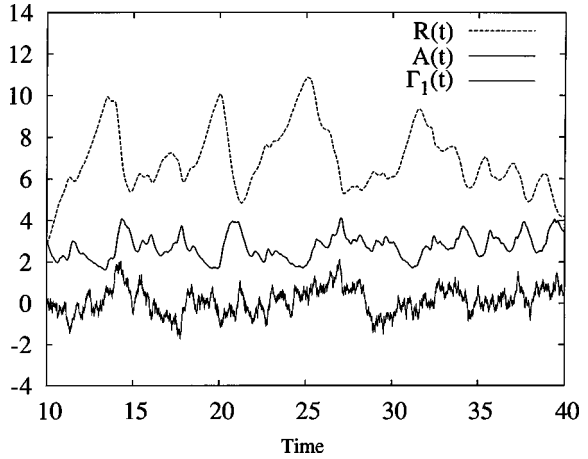

FIG. 6. Time evolution of sample flame-ball radius (R), heat-loss function (A), and first reduced rate-of-strain $\Gamma_1(u)$ for $\mu=5$ and $\tau=100$. Notice that R and A are anticorrelated, whilst the correlation between A and $|\Gamma_1|$ is positive at large $|\Gamma_1|$'s.

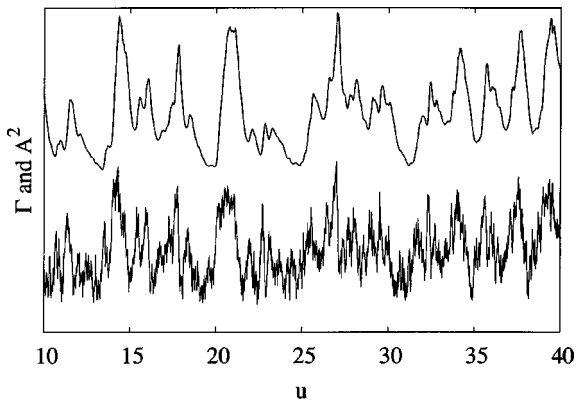

FIG. 7. Sample squared heat-loss function A^2 (top) and total rate-of-strain $\Gamma \equiv [\Gamma_1^2+\Gamma_2^2+\Gamma_3^2]^{1/2}$ (bottom) vs time u. Notice the positive correlation between both functions, and the small delay (A^2 is late) between them. (To ease readibility, each curve has a different vertical scale.)

$\exp(-|u-u'|)$ as autocorrelation function, that of $A^2 - \langle A^2 \rangle$, $\mathcal{G}_{A^2}(\xi \equiv |u-u'|)$ is more regular at $u \sim u'$. (See also Fig. 7.) The autocorrelation function $\mathcal{G}_{A^2}(\xi)$ turns out to be almost undistinguishable (see Fig. 8) from

$$\mathcal{G}_{A^2}(\xi) = \mathcal{G}_{A^2}(0)\,\frac{\mu \exp(-\nu\xi) - \nu \exp(-\mu\xi)}{\mu - \nu}, \qquad (36)$$

with $\nu \simeq 2$ and $\mathcal{G}_{A^2}(0) = O(\mu)$ for large enough μ's. The corresponding spectral "energy" density $\mathcal{S}(\omega)$ is then proportional to $\mu/(1+\omega^2/\nu^2)(1+\omega^2/\mu^2)$. Put in words, $\mathcal{G}_{A^2}$ happens to nearly coincides with the normalized autocorrelation function $\mathcal{G}_\Gamma$ of $\Gamma - \langle \Gamma \rangle$, provided the Γ_i's are filtered with an $O(\mu)$ cutoff frequency, a process henceforth designated as "μ filtering," otherwise, $\mathcal{G}_\Gamma(\xi)$ turns out be very close to $\exp(-\nu|\xi|)$. Strictly speaking one should distinguish a total strain deduced from μ-filtered Γ_i's, from a μ-filtered Γ; numerical simulations gave us ample evidence that the difference is immaterial when μ is large enough.

That such a simple fit as Eq. (36) works so well is surprising, in view of the nonlinear operations (22) and (23) needed to get $A(u)$ from the $H_i(u)$; anyway, this is compatible with an $O(1/\mu)$ range of memory effects.

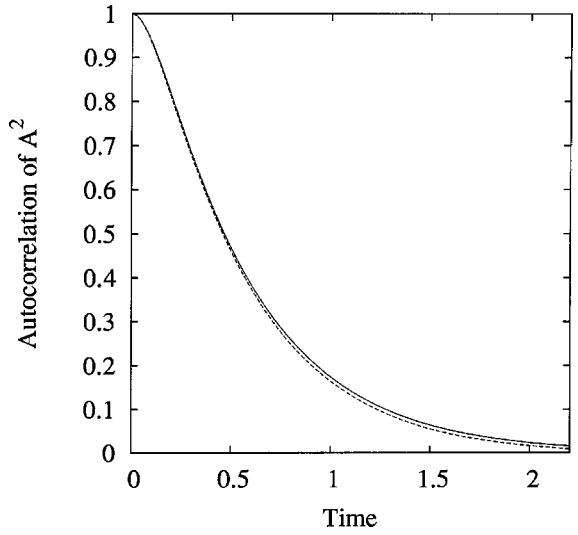

FIG. 8. Numerical autocorrelation function $\mathcal{G}_{A^2}(\xi)$ of the squared heat-loss function A^2 (dashed line) for $\mu = 9$. The solid line represents the fitting function [see text, Eq. (36)]. The agreement is even better for $5 \leqslant \mu < 9$.

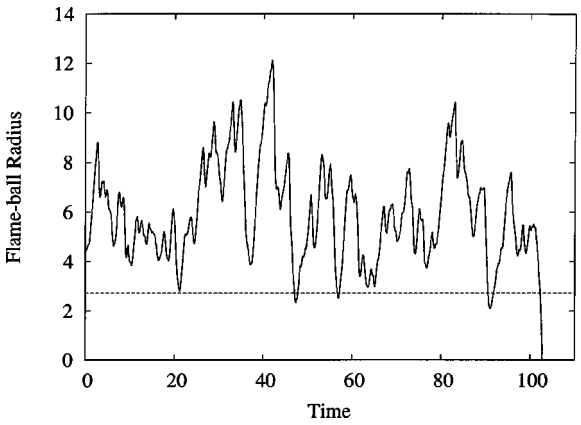

FIG. 9. Sample time evolution of a flame-ball radius $\mathcal{R}$. The FB radius shrinks to zero (extinction) at a finite time. The dashed horizontal line represents $R = e$, which $\mathcal{R}(u)$ occasionally crosses for a short while.

B. FB-radius trajectories and statistics of lifetimes

As illustrated in Fig. 9, a flame ball cannot live for infinitely long; $\mathcal{R}(u)$ eventually shrinks to zero at some finite time u_{life}, that depends on the parameters τ [Eq. (21)], μ [Eq. (17)], and on the specific realization of the $H_i(u)$'s.

Figure 10 shows histograms of u_{life} at fixed values of μ (=5) and τ (=100), and for many (=2992) realizations of the $H_i(u)$'s. Let $\langle u_{life} \rangle$ denote the ensemble average of the u_{life}'s; as shown in Fig. 10, the fit

$$\Pi(u_{life}) = \frac{1}{\langle u_{life} \rangle} \exp\left(-\frac{u_{life}}{\langle u_{life} \rangle} \right) \qquad (37)$$

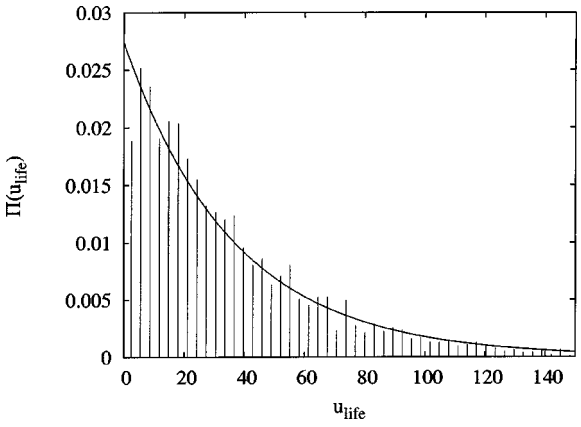

FIG. 10. Numerical probability density function of lifetimes $\Pi(u_{life})$ for $\mu = 5$ and $\tau = 100$ (vertical bars). The solid curve is the exponential fit given by Eq. (37). The finite duration of the FB quenching process is visible at small u_{life}'s.

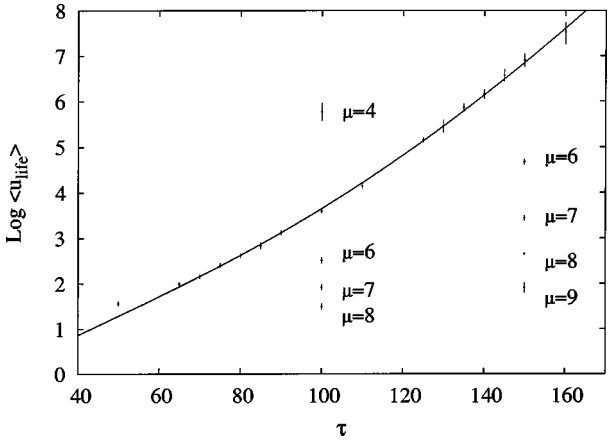

FIG. 11. Ensemble-averaged lifetime $\langle u_{life}\rangle$ as a function of parameter τ, for $\mu=5$ (symbols) and corresponding fitting curve [solid line, Eq. (38)]. The $\langle u_{life}\rangle$'s corresponding to $\tau=100$ and 150 and the listed different μ's are also represented. The error bars resulting from the finite number of realizations are given by the height of the symbols.

satisfactorily represents the Pdf $\Pi(\cdot)$ of u_{life}, as soon as u_{life} exceeds 2–5. The variations of $\langle u_{life}\rangle$ with τ for $\mu=5$ are shown in Fig. 11 (some computed $\langle u_{life}\rangle$'s for other μ's and for $\tau=100$ and 150 are also displayed). For $\mu=5$, it turns out for that the results can be accurately fitted by

$$\langle u_{life}\rangle = \exp(a(\tau-b)^2 + c\log\tau + C), \tag{38}$$

with $a=(k/\mu J)^2$, $J\simeq 17$, $k=1.275$, $b\simeq 0$, $c=1$, and $C=-3.185$ [28].

The very fast growth of $\langle u_{life}\rangle$ with τ, at fixed μ, is worth noticing: for $\mu=5$, we could not make statistically significant calculations beyond $\tau=160$, in which case $\langle u_{life}\rangle$ is of about 1850 and requires several weeks of CPU for 110 runs on a 2.4 GHz PC. Besides, $\langle u_{life}\rangle$ decreases rapidly as μ increases, especially at large τ's (see Fig. 11).

C. Explicitly-filtered noises

To evaluate the influence of the smoothness of the random entries, we repeated the above procedure, replacing the Ornstein-Uhlenbeck processes H_i's by more regular ones now denoted h_i's. To this end, we applied a first-order low-pass filter, with a unit cutoff time, to the H_i's before calculating the Γ_i's (then denoted γ_i's). The ODE's for the h_i's are

$$\dot{h}_i = -\frac{h_i}{1} + \sqrt{2}H_i, \tag{39}$$

where $\dot{h}_i \equiv dh_i/du$ and the piecewise linear H_i's are still computed according to Eq. (19); to ensure that the h_i's (or the χ_i's evoked below) have the correct regularity at the mesh points, the numerical code was provided with analytical integration formulas for $h_i(u_{n+1})-h_i(u_n)$. Equations (39) being linear, the h_i's they define are still centered Gaussian processes, with $\langle h_i^2\rangle=1$. Their common autocorrelation function is $\mathcal{G}_h(\xi)\sim(1+|\xi|)\exp(-|\xi|)$, the corresponding spectral density being $\sim(1+\omega^2)^{-2}$. The resulting $\langle u_{life}\rangle$ is exhibited in Figs. 12 and 13 as a function of τ, μ. Interestingly, the fitting curve *again* is given by Eq. (38), yet with $k=1$; parameter C is now -2.85 instead of -3.185; parameters b and c have the same numerical values of 0 and 1, respectively.

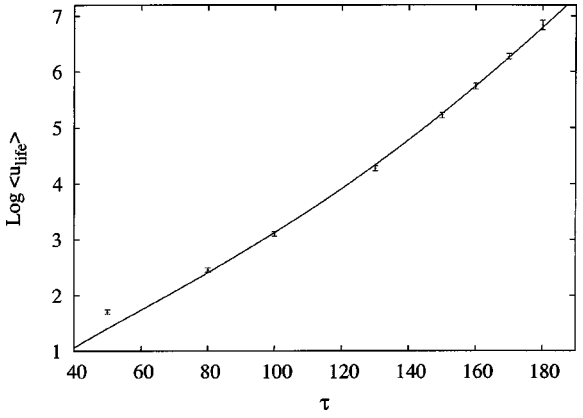

FIG. 12. Ensemble-averaged lifetime $\langle u_{life}\rangle$ as a function of parameter τ, for $\mu=5$ and explicitly filtered stimuli, and corresponding fitting curve [solid line, Eq. (38) with $k=1$ and $C=-2.85$]; compare to Fig. 11. The error bars resulting from the finite number of realizations are given by the height of the symbols.

Going one crank further, i.e., defining χ_i's from the h_i's by equations similar to Eq. (39) (with the last term replaced by $h_i\sqrt{4/3}$ to ensure $\langle\chi_i^2\rangle=1$), did not change the above fit of $\langle u_{life}\rangle$ significantly, even though each χ_i's spectral power density is now $\sim(1+\omega^2)^{-3}$.

VI. TENTATIVE INTERPRETATIONS

A. PDF of lifetimes

Because of the very structure of Eq. (24), the response of $\mathcal{R}(u)$ to the fluctuating heat-loss function (A or $\tilde{A}$) is not local in time. However, the fast decay of $\Delta^{-1/2}(u,v)$ with increasing $u-v$ implies a localized response: only the im-

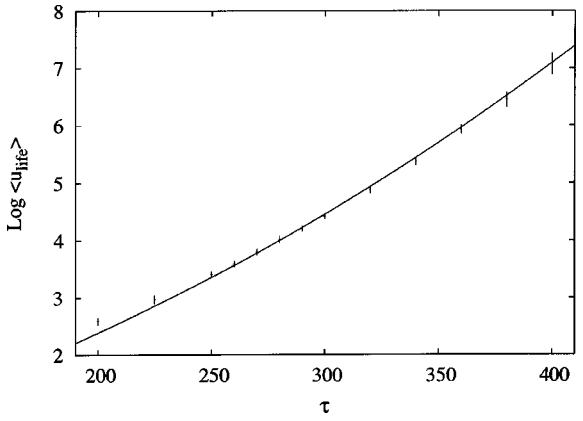

FIG. 13. Ensemble averaged lifetime $\langle u_{life}\rangle$ as a function of parameter τ, for $\mu=10$, and corresponding fitting curve [solid line, Eq. (38) with $k=1$ and $C=-4.1$], for explicitly filtered stimuli. The error bars, due the finite number of realizations, are given by the height of the symbols.

mediate past $u-v \ll 1$ matters. As a consequence, one may admit that a localized criterion for extinction would exist; the latter will depend on τ, μ and $A(u)$ in some neighborhood $[\leqslant O(1)]$ of the times it is met, but, on average, not on the precise times this occurs, if the possibility is a rare event.

Let $1/\mathcal{U}$ be the average rate at which this may occur (we implicitly assume $\mathcal{U} \gg 1 \equiv$ the correlation time of the H_i's). Since a flame ball extinguishes only once, $\Pi(u_{life})du_{life}$ is the probability that the extinction criterion would be fulfilled in the interval $[u_{life}; u_{life}+du_{life}[$ *for the first time*; accordingly $\Pi(u_{life})$ must satisfy

$$\Pi(u_{life})du_{life} = \left(1 - \int_0^{u_{life}} \Pi(u)du\right)\frac{du_{life}}{\mathcal{U}}, \qquad (40)$$

the first factor in the RHS expressing that extinction did not take place prior to u_{life}. Equation (40) yields $\Pi(u_{life})$ in the same form as Eq. (37), provided $\langle u_{life}\rangle \equiv \mathcal{U}$: $1/\langle u_{life}\rangle$ is thus identified with the probability per unit time (PUT) $1/\mathcal{U}$, assumed to be independent [29] of u_{life}, that the extinction criterion be met by $A(u)$ [30]. Note that the rms fluctuation of u_{life} about $\langle u_{life}\rangle$ is $\langle u_{life}\rangle$ itself when Eq. (37) holds. The error bars in Figs. 11–13 merely correspond to the uncertainty $(\sim \langle u_{life}\rangle/\sqrt{N})$ on $\langle u_{life}\rangle$ brought about by the number N of numerical runs being finite.

B. Dependence of $\langle u_{life}\rangle$ on noise properties

The foregoing tentative interpretation of Eq. (38) rests on a result established by Rice [15] and Kac [16]: the probability $1/\mathcal{U}$ per unit time that a stationary random process $X(u)$ would cross a threshold X_{crit} satisfies

$$\frac{1}{\mathcal{U}} \sim \int_{-\infty}^{+\infty} |\dot{X}|\Pi(X_{crit}, \dot{X})d\dot{X}, \qquad (41)$$

where $\Pi(X,\dot{X})$ is the joint probability density of X and $\dot{X} \equiv dX/du$. Whenever the crossing is a rare event, e.g., when X_{crit} lies in the tail of the PDF of X, Eq. (41) also gives the PUT that $\max(X) \geqslant X_{crit}$, up to a factor of 1/2. Our present strategy is to try and apply Eq. (41) to $X = A^2(u)$ assuming that the criterion for FB extinction would correspond to $A^2 > A^2_{crit}$; a way of estimating A^2_{crit} itself is presented in Appendix A.

Relating $A(u)$ to the $\Gamma_i(u)$'s

The above approach first requires to relate the statistics of $A(u)$ to the $\Gamma_i(u)$'s that generate it. The way the integrand appearing in Eq. (23) varies with $u-v$ and u (cf. Fig. 15) makes it clear that the heat-loss function $A(u)$ becomes larger whenever $1/\Delta^{1/2}(u,v)$ fades over a shorter $u-v$ lapse of time. Inspection of Eq. (22) reveals that at least one of the $|2\mu\Gamma_i|$'s must get momentarily large to achieve this. Generically this occurs when $2\mu \gg 1$ (a reasonable assumption since $2\mu = 10-20$) and/or one [31] of the $|H_i|$'s (or h_i or χ_i in the explicitly filtered cases) noticeably exceeds their common rms value; in the latter instance the $|\mu\Gamma_i|$'s are in the ratios 1:1/2:1/2 [see Eq. (18)] within $O(1/\mu\Gamma)$ fractional errors, with $\Gamma(u)$ defined by Eq. (27). In the formal limit $\mu \to +\infty$ we exploit here, only the immediate past $0 < u-v \sim 1/\mu$ significantly contributes to the dependency of $A(u)$ on the $\Gamma_i(u)$'s. We then expand the inner integrals in Eq. (22) as

$$\mu \int_u^w \Gamma_i(\xi)d\xi = \mu\Gamma_{i*}(u)(w-u) + O(\dot{\Gamma}_{i*}(u)\mu(w-u)^2). \qquad (42)$$

In Eq. (42), $\Gamma_{i*}(u)$ stands for $\Gamma_i(u)$ once averaged over an $O(1/\mu)$ interval of time preceding u and hence represents Γ_i evaluated at some u_* in this interval $[0 < u-u_* = O(1/\mu)]$. The averaging brings about an $O(\mu)$ upper cutoff frequency, and hence reduces the rms value of the Γ_{i*}'s below $(2/3)^{1/2}$ by an $O(1/\mu)$ amount, since the Γ_i's spectral power density decreases like ω^{-2} at high frequencies ω.

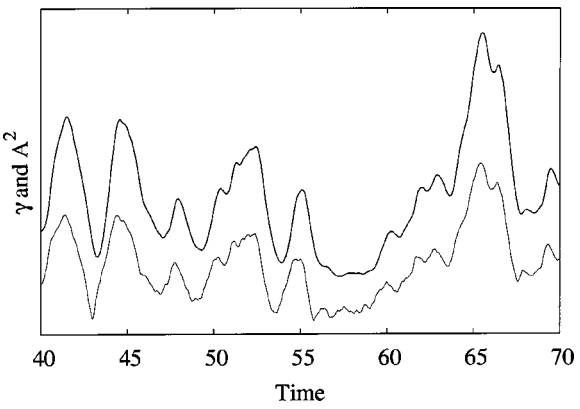

FIG. 14. Sample squared heat-loss function A^2 (top; thick line) and total rate-of-strain $\gamma \equiv [\gamma_1^2+\gamma_2^2+\gamma_3^2]^{1/2}$ (bottom; thin line) in the filtered-noise case. The correlation between A^2 and γ is more apparent than in Fig. 7. Some filtering still exists between γ and A^2, and the latter is again slightly late with respect to $\gamma(u)$. (As in Fig. 7, each curve was scaled differently to ease readibility.)

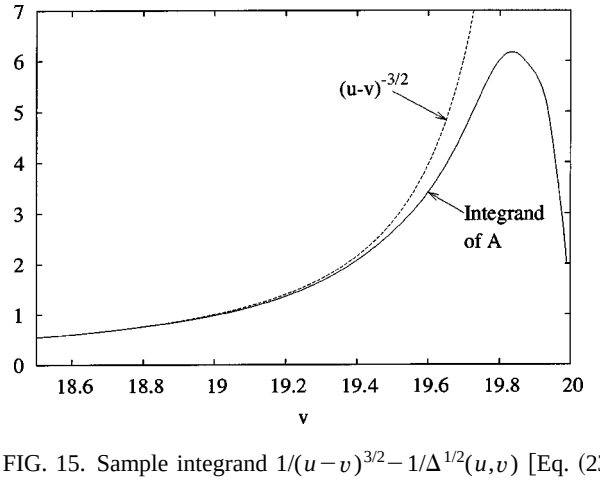

FIG. 15. Sample integrand $1/(u-v)^{3/2} - 1/\Delta^{1/2}(u,v)$ [Eq. (23)] of the scaled heat-loss function $A(u)$, as a function of v, for a fixed time $u=20$ and for $\mu=5$. Note the maximum at $\mu(u-v) \simeq 1$.

Next, performing the outer integrals in Eq. (22) produces to leading order the same $I(\Gamma_{1*},\Gamma_{2*},\Gamma_{3*})$ as in Eq. (24), now evaluated in terms of the $\Gamma_{i*}(u)$. Employing Eq. (28), one gets (see Figs. 7 and 14).

$$\frac{A^2(u)}{\mu\sqrt{\frac{8}{3}}} \simeq \Gamma_*(u) + \varepsilon(u), \tag{43}$$

with a delayed and filtered total strain $\Gamma_*(u)$ defined analogously to Eq. (27). The term $\varepsilon(u)$ in Eq. (43), stemming from the RHS in Eq. (42), is certainly nonnegative for $A(u)$ may vanish if and only if all the Γ_i's identically do, and is formally $o(1)$ in the limit $\mu\to\infty$. More precisely,

$$\varepsilon(u) \sim \sum_i b_i(\Gamma_{i*},\Gamma_{2*},\Gamma_{3*}) \frac{\dot{\Gamma}_{i*}}{\mu\Gamma_{i*}}, \tag{44}$$

with $b_i = O(1)$.

As an attempt to reduce the influence of $\varepsilon(u)$ in Eq. (43), and better specify the aforementioned delay $u-u_*$, we chose to make the approximation that the Γ_{i*}'s would satisfy

$$\frac{\alpha}{\mu}\dot{\Gamma}_{i*} = -\Gamma_{i*} + \Gamma_i, \quad 0 < \alpha = O(1). \tag{45}$$

Compatibility with Eq. (36) then required $\alpha \simeq 1$ once Eq. (43), with $\varepsilon(u)$ neglected, is made use of. We are fully aware that a more sensible modeling of the μ-filtering process would employ $\alpha/\mu\Gamma_*$ as cutoff time; the consequences of Eq. (45) are therefore expected to be correct only qualitatively. The main virtue of Eq. (45) is linearity, however: the Γ_{i*}'s are still Gaussian, with rms values of $(2/3(1+2/\mu))^{1/2}$ and the joint PDF $\Pi(\Gamma_*,\dot{\Gamma}_*)$ for the corresponding total strain Γ_* and $\dot{\Gamma}_* \equiv d\Gamma_*/du$ is then accessible analytically (Appendix B). In particular, integration of $\Pi(\Gamma_*,\dot{\Gamma}_*)$ with respect to the last variable, then the use of Eq. (43), produces the following PDF for A^2:

$$P_{A^2}(A^2) \sim \frac{A^2}{\mu} \exp\left(-\left(\frac{A^2}{4\mu/\sqrt{3}} \right)^2 \left(1 + \frac{2}{\mu} \right) \right). \tag{46}$$

Figure 16 compares the numerically computed PDF of A^2/μ to Eq. (46), for different values of μ. The predicted trend is correct and improves as μ increases, as expected. Next, merely replacing $k'^2 \equiv (1+2/\mu)$ by $(1+0.4/\mu)$ in Eq. (46) produces a much better fit of the numerics (see Fig. 16), especially for A^2/μ above 2 (for $\mu=5$) or 1 (for $\mu=9$). Very plausibly, this is so because the actual μ filtering has an $O(1/\mu\Gamma_*)$ cutoff time instead of $1/\mu$.

Mean FB lifetime vs A_{crit}

Employing $\Pi(\Gamma_*,\dot{\Gamma}_*)$, deduced in Appendix B when Eq. (45) holds, and Eq. (43) (with ε neglected) in the Rice-Kac formula (41) gives the estimate

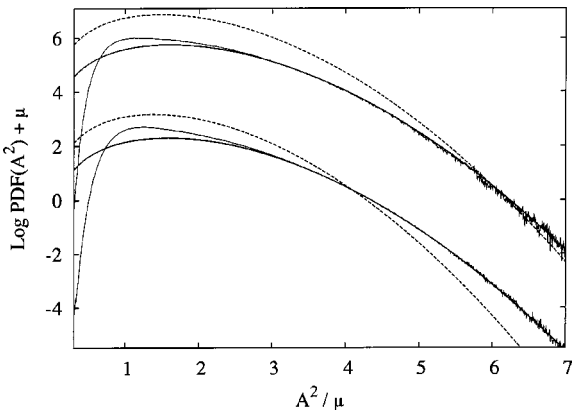

FIG. 16. Probability density functions of A^2 for $\mu=5$ (bottom) and $\mu=9$ (top) as a function of A^2/μ. (To ease readability, we artificially shifted the curves.) The fitting curves are proportional to $A^2/\mu \times \exp -(A^2/\mu)^2/2\sigma^2$, with $\sigma^2 = 8/3\times(1+2/\mu)^{-1}$ (dashed lines) and $\sigma^2 = 8/3\times(1+0.4/\mu)^{-1}$ (thick solid lines). Notice that the quality of the fits improves as μ grows.

$$\frac{1}{\langle u_{life}\rangle} \sim \mu^{1/2} \frac{A_{crit}^2}{\mu} \exp\left[-\left(\frac{k' A_{crit}^2}{4\mu/\sqrt{3}} \right)^2 \right] \tag{47}$$

for $\langle u_{life}\rangle = \mathcal{U}$ corresponding to a presumed A_{crit}. Recall that the $\mu^{1/2}$ factor in Eq. (47) comes from the $O(\mu)$ upper cutoff frequency brought about by the averaging over $u-v = O(1/\mu)$ in Eq. (43); and $0 < k'^2 - 1 = O(1/\mu)$ comes from the frequencies over $O(\mu)$ having been filtered out from Γ_i's that have $\sim\omega^{-2}$ power spectral densities at $\omega \gtrsim O(1)$.

Mean FB lifetime

Appendix A provides one with

$$A_{crit}^2 \simeq \tau e^{-2}(1+\eta) + O\left(\frac{\eta^2\tau}{4e^2} \right), \tag{48}$$

in the situations where $\mu \gg 1$ and $\tau \gg 1$ and the H_i's are not filtered explicitly; in Eq. (48), $0 < \eta \lesssim O(\mu^{2/5}\tau^{-4/5})$ or $O(\mu^{3/7}\tau^{-4/7})$ depending on whether $\mu^4 \ll \tau^3$ or $\mu^4 \gg \tau^3$, respectively (up to numerical factors), and $0 < \eta \lesssim O(\tau^{-1/2})$ at crossover $\mu^4 \sim \tau^3$.

From Eqs. (47) and (48), our theoretical estimate of the mean flame-ball lifetime is of the form

$$\langle u_{life}\rangle \sim \mu^{-1/2} \left(\frac{\mu}{\tau-\beta} \right)^c \exp\left[\left(\frac{k(\tau-\beta)}{4\mu e^2/\sqrt{3}} \right)^2 \right] \tag{49}$$

in that case. In Eq. (49), $c=+1$, $k = k'(1+\eta) > 1$ and $\beta = O(\eta^2\tau/4)$.

Comparison with numerics

The above prediction has the same functional form as Eq. (38), with $a = k/\mu J$, $J = 4e^2/\sqrt{3} \simeq 17.06$, $k>1$ and $b \simeq 0$. Whereas our analyses give no numerical estimate of $\eta \ll 1$, Eq. (49) is compatible with Eq. (38), especially in view of the computational constraints that prevented us from exploring very large values of τ and/or μ. Yet it is astonishing that

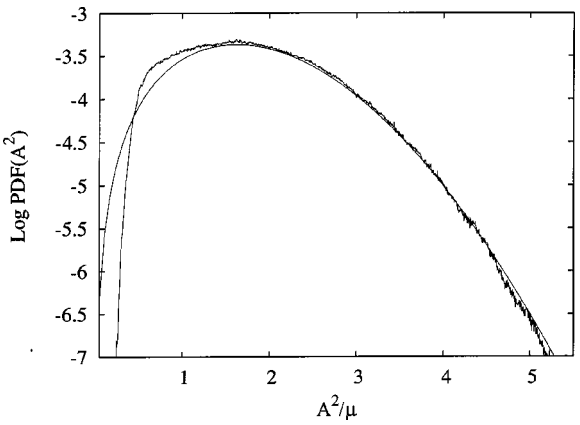

FIG. 17. Probability density function of A^2 for $\mu=10$ as a function of A^2/μ, for the filtered Ornstein-Uhlenbeck processes [Eq. (39)]. The smoother line represents the fitting curve: $A^2/\mu\times\exp -(A^2/\mu)^2/2\sigma^2$, with $\sigma=\sqrt{8/3}$.

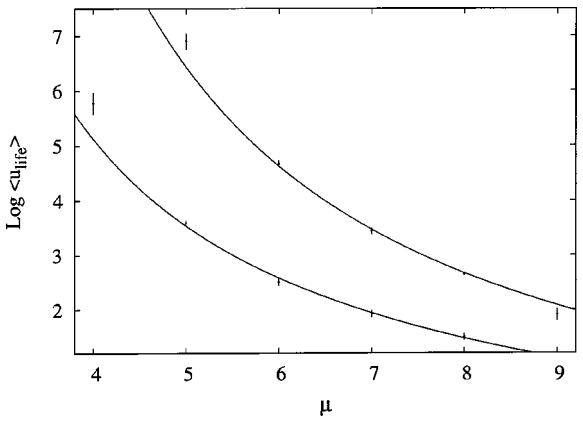

FIG. 18. Ensemble averaged lifetime $\langle u_{life}\rangle$ as a function of parameter μ for Gaussian noises for $\tau=100$ (bottom) and $\tau=150$ (top), and corresponding fitting curve (solid lines); see Eqs. (38) and (49) and also Fig. 12. The error bars, due the limited number of realizations, are given by the height of the symbols.

the fit (38) of the numerical $\langle u_{life}\rangle$'s is compatible with the functional form (49)... with $c=-1$ instead of $+1$; we could not explain the discrepancy.

In the case of Gaussian stimuli $h_i(u)$, that are explicitly filtered once [Eq. (39)], an $O(1/\mu)$ time lag between A^2 and γ still exists (see Fig. 14), but the k' factor should be—and indeed is—absent from the coefficient a in Eq. (38), because μ filtering does not remove any significant energy from the γ_i's, the spectral power of which now decays as ω^{-4} at high frequencies. This is confirmed by the comparison of Eq. (46) with the computed PDF of A^2 at large μ (see Fig. 17). Also the $\mu^{1/2}$ factor should, and does, disappear from Eq. (47), since the γ_i's are differentiable even without the μ filtering brought about by Eq. (23); finally, as indicated by Eq. (A12), η is now typically $\leqslant O(1/\tau)$, whereby $k\simeq 1$ in Eq. (49). This is still perfectly compatible with the numerics (see Sec. V C)... were it not for the fact that the exponent c in the prefactor of Eq. (49) needs again to be -1 instead of $+1$.

We numerically checked that employing stimuli that are explicitly filtered twice (the χ_i's evoked at the end of Sec. V C) did not change the $\langle u_{life}\rangle$ values any further, consistently with our interpretation that $k'-1$ and η [see Eq. (A11)] are then even smaller [$\mathcal{S}(\omega)\sim\omega^{-6}$]. Yet $c=1$ still has to be replaced by -1.

Equation (49), with $c=-1$, also correctly predicts the dependency of $\langle u_{life}\rangle$ on μ, at fixed τ, as evidenced in Fig. 18.

C. Non-Gaussian stimuli

The dependency of $\langle u_{life}\rangle$ on τ and μ relies on the Gaussian characteristics of the H_i's. This begs the question of how would the FB mean lifetime be modified upon replacing Eq. (19) by

$$\frac{H_i(u_{n+1})-H_i(u_n)}{\delta u}=-\left.\frac{\partial V}{\partial H}\right|_{H=H_i(u_n)}+\varepsilon_i^n\kappa(\delta u), \quad (50)$$

with the same $\kappa(\delta u)$ as in Eq. (19), but with a potential $V(H)$ different from the previous $H^2/2$. Specifically, we assumed

$$V(H)=\log\left(2\cosh\left(\frac{\pi}{2}H\right)\right) \quad (51)$$

whereby the H_i's have the new PDF

$$P_H(H_i)=\frac{1}{2}\,\frac{1}{\cosh\left(\frac{\pi}{2}H_i\right)} \quad (52)$$

and hence still satisfy $\langle H_i\rangle=0$, $\langle H_i^2\rangle=1$. Gaussian processes are definitely different, and employing Eq. (51) raises new difficulties, that are evoked below.

Even in absence of any filtering, we could not determine the joint PDF of each pair $(H_i,\dot{H}_i)$ that is no longer a multivariate Gaussian. This prevented us from evaluating $\Pi(\Gamma,\dot{\Gamma})$ and the integrand in Eq. (41). We propose the estimate

$$\int_{-\infty}^{+\infty}|\dot{\Gamma}|\Pi(\Gamma_{crit},\dot{\Gamma})d\dot{\Gamma}\sim P_\Gamma(\Gamma_{crit})\langle(\dot{\Gamma})^2\rangle^{1/2}, \quad (53)$$

guided by the integrand in Eq. (41) being non-negative and by the identity $P_\Gamma(\Gamma)\equiv\int_{-\infty}^{+\infty}\Pi(\Gamma,\dot{\Gamma})d\dot{\Gamma}$. This is an exact result for Gaussian H_i's (see Appendix B). Put in words, Eq. (53) neglects any conditioning of $\dot{\Gamma}$ on Γ.

Unfortunately, even deriving $P_\Gamma(\Gamma)$ analytically is marginally easy when Eq. (51) holds; still, it is found (see Appendix C) that $P_\Gamma(\Gamma\to 0)\sim\Gamma$ and, more importantly,

$$P_\Gamma(\Gamma\to+\infty)\sim\exp\left(-\frac{\pi\sqrt{6}}{4}\Gamma\right) \quad (54)$$

to be compared with $P_\Gamma(\Gamma\to+\infty)\sim\Gamma\exp(-\Gamma^2/2)$ in the Gaussian case. In the presence of a linear filtering of the H_i's

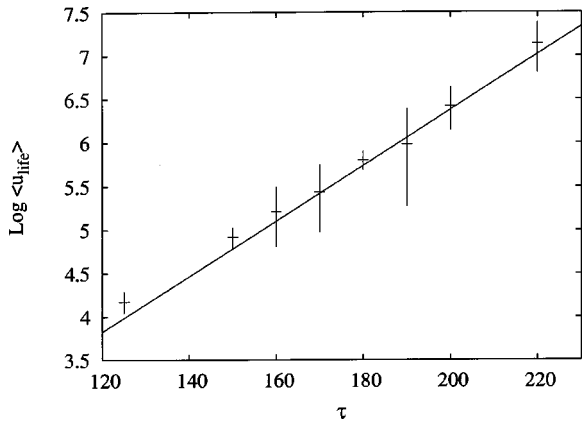

FIG. 19. Ensemble averaged lifetime $\langle u_{life}\rangle$ as a function of parameter τ for non-Gaussian noises, for $\mu=5$, and corresponding fitting curve [solid line, Eq. (55) with $\eta=0$]. The error bars, due the finite number of realizations, are given by the height of the symbols.

with an $O(\mu)$ upper cutoff frequency, the RHS values of the H_i's are still reduced by a factor $[1+O(1/\mu)]$ (previously denoted k' in the Gaussian case), again because Eq. (50) is a first-order Markov process, implying spectral power densities that decay like ω^{-2} at large frequencies. Working along the same line—via Eqs. (43), (48), and (54)—as that leading to Eq. (49) in the Gaussian case, our new prediction on the FB lifetime is thus

$$\langle u_{life}\rangle \sim \mu^{-1/2}\exp\left[\sqrt{\frac{3}{8}}\frac{\pi\sqrt{6}}{4e^2}(1+\eta)\frac{\tau}{\mu}\right], \qquad (55)$$

in absence of explicit filtering. The predicted linear dependency of $\log\langle u_{life}\rangle$ on τ/μ, and the slope (with $\eta\ll 1$), are consistent with our numerical findings plotted in Fig. 19.

VII. CONCLUDING REMARKS

The evolution equation (20) constitutes a rather unusual dynamical system. It indeed simultaneously involves: a logarithmic nonlinearity, a stochastic multiplicative forcing $A(u)$ that is not white in time, and memory effects with a kernel related to $A(u)$ in a nontrivial way through Eqs. (22) and (23). None of such peculiarities can be eliminated. The $\log(\cdot)$ term comes from the highly convex—but unavoidable, Arrhenius factor in Eqs. (3) and (4); $A(u)$ is autocorrelated in time because the Lagrangian velocity gradient **g** is; the determinant of the b_{ij}'s and the memory kernel are related to the heat-loss function A because all originated from the past history of a FB being stored diffusively in temperature and mass fraction fields around it; and $A(u)$ acts as a factor in Eq. (20) because the far-field equations always are linear, yielding Eqs. (13) and (14). Very plausibly, the attractive features are not alien to the difficulties we met when trying to evaluate the reduced mean flame-ball lifetime $\langle u_{life}\rangle$ analytically. Only for quasisteady ($\tau\gg 1$), yet significant ($\mu\gg 1$), forcings could the memory effect be considered short-ranged and a simple link between total strain (Γ) and forcing function $A(u)$ be identified. Then numerics and tentative interpretation agree that (i) the statistics of FB lifetimes (t_{life}) is of the Poisson type; (ii) the mean lifetime $\langle t_{life}\rangle \equiv \tau\langle u_{life}\rangle\ t_Z$ may considerably exceed the time t_Z of spontaneous FB evolutions; (iii) the variations of $\langle u_{life}\rangle$ with the properties of **g** fairly mirror the latter's statistics, essentially because individual FB extinctions probe the intermittency of the velocity gradients.

Admittedly this was obtained for diagonal **g**'s, and several generalizations of the results presented here must be worked out before any comparison with experiments is attempted: accounting explicitly of a FB ignition instead of the switch-on procedure adopted here, incorporating the effects of nondiagonal traceless **g**'s, handling collective effects.

Nondiagonal, yet still symmetric, Lagrangian velocity gradients $\mathbf{g}(\cdot)$ should not pose major problems: the kernel storage trick summarized in Eqs. (30) and (31) can be generalized to any **g**, and the approximation leading to Eq. (43) is amenable to a simple generalization, because **g** may be assumed nearly diagonal about the current time u: the squared total strain Γ^2 is then identified with $\mathrm{trace}(\mathbf{g}^2)\geqslant 0$.

Purely antisymmetric **g** apparently is not a difficult case either: $g_{ij}=-g_{ji}$ in Eq. (15) produces $b_{ij}=(t-s)\delta_{ij}$, then $A(u)\equiv 0$ and $\Delta(u,v)=(u-v)^3$, since rotating a spherically symmetric FB does not change its dynamics from the spontaneous one. Yet, difficulties would then be encountered about the switch-on procedure, because the FB spontaneous dynamics only has $\mathcal{R}=0$ and $\mathcal{R}\to+\infty$ as stable attractors [9]. This extreme situation points to the need for equipping Eq. (20) with some mathematical device [namely, a positive term $\sqrt{\tau}f(u)/\mathcal{R}$ added to the rhs of Eq. (20)] [9] so as to trigger the growth of $\mathcal{R}(u)$ from zero at $u=0$.

Handling g_{ij}'s that have no special symmetry poses no major numerical difficulty, but making analytical predictions about them is notoriously difficult [17]: $\mathbf{g}(t)$ may occasionally have a pair of complex-conjugate eigenvalues and the required generalization of $A^2/gm\sim\mathrm{trace}(\mathbf{g}^2)$ is not patent. Furthermore, it is not obvious at all which constraints on **g**, apart from tracelessness, need be imposed to ensure that the Lagrangian rate-of-strain tensor actually follows from the incompressible Navier-Stokes equations [18].

Finally, the mean field approach taken up in [19] may prove useful to mimic a "gas" of flame balls that are mutually interacting through conductive/diffusive processes; this would give access to the corresponding regime of "spotty" turbulent combustion of mobile gaseous fuels. Yet the very notion of a "mean-field" interaction requires a "sum over all $g_{ij}(t)$ histories," a difficulty of its own [20]. All this is under study.

Of course experiments would be welcomed, e.g., upon firing a spark at the center of a spherical bomb of radius L filled with the gaseous premixture and where turbulence is sustained by spinning fans. Yet the following difficulty must not be forgotten: since the flame ball center essentially executes a Brownian motion, it may approach the bomb wall within an $O(\mathrm{Ze}\,r_Z)$ distance after a time $\sim L^2/D_{turb}$ — where $D_{turb}\equiv$ turbulent diffusivity — which can induce FB premature extinction [22] whenever L^2/D_{turb} is not very large compared to the expected $\langle t_{life}\rangle$.

APPENDIX A: ON THE EXTINCTION CRITERION

When $A(u)/\sqrt{\tau}$ is $O(1)$ and τ is large enough, we anticipate that the variations of $\mathcal{R}(\cdot)$ remain $O(1)$ over an $O(1)$ interval of time $u-v$. The LHS of Eq. (20) may then be treated as a perturbation of $A(u)/\sqrt{\tau}=\log\mathcal{R}/\mathcal{R}$. This perturbation is singular if $A(u)\leqslant O(1)$, i.e., most of the time unless μ is also large, which we assume: the rapid decrease of $1/\Delta^{1/2}(u,v)$ for $\mu(u-v)\sim O(1)$ then allows one to write

$$\frac{1}{\sqrt{\tau}}\int_{-\infty}^{u}\frac{\mathcal{R}(u)-\mathcal{R}(v)}{\Delta^{1/2}(u,v)}dv\simeq\frac{\varphi(u)}{\sqrt{\tau}}\frac{d\mathcal{R}}{du}, \tag{A1}$$

$$\varphi\equiv\int_{-\infty}^{u}\frac{(u-v)}{\Delta^{1/2}(u,v)}dv. \tag{A2}$$

The function $\varphi(u)$ generically is $\leqslant O(\mu^{-1/2})$. Note that, when $\mu\gg 1$ and Eq. (43) holds, $\varphi(u)$ happens to be very close to the formula

$$\varphi(u)\simeq\mu^{-1/2}\Gamma_{*}^{-1/2}(u)\sqrt{2}\left(\frac{\pi}{2}+\log 2\right), \tag{A3}$$

which is actually exact in the steady case and when the $|\Gamma_{i*}|$'s are in the ratios 1:1/2:1/2. One then deduces $\varphi(u)A(u)\simeq(2/3)^{1/4}(\pi+2\log 2)\equiv\lambda$, an approximation we shall adopt here.

The aforementioned perturbation scheme also fails when $A(u)/\sqrt{\tau}$ approaches e^{-1}, because $d\mathcal{R}/du$, as predicted by a quasisteady analysis, becomes too large to be neglected: a temporal boundary layer exists around some $u=u_0$ (say), where $\mathcal{R}(u)\simeq e$ and $A(u)/\sqrt{\tau}\simeq e^{-1}$ [whence $\varphi\simeq\lambda/(e^{-1}\sqrt{\tau})$]. We anticipate that the approximation (A1) and (A2) still holds. Expanding Eq. (20) for $\mathcal{R}\simeq e$ produces a Riccati ODE to leading order:

$$\frac{\lambda}{\tau}\frac{d(\mathcal{R}-e)}{d(u-u_0)}\simeq-\frac{(\mathcal{R}-e)^2}{2e^3}-\left(\frac{A(u)}{\sqrt{\tau}}-e^{-1}\right), \tag{A4}$$

to be solved with the ''initial'' condition that its solution $\mathcal{R}-e$ would match the quasi-steady response soon enough before $u=u_0$. For $u-u_0>0$ and large enough, two extreme possibilities exist: either $\mathcal{R}-e$ decreases towards $-\infty$, shortly leading to extinction, or $\mathcal{R}-e$ ultimately resumes another phase of quasisteady behavior. The extinction criterion we are looking for corresponds to the properties that $A(u)$ must fulfill around $u=u_0$ for the separatrix trajectory to be observed. Clearly, $A(u)$ must be close to a maximum, in some sense. Everything depends on the precise shape of $A(u)$ about u_0. In a rough approximation, we assume that $A(u)\simeq A(u_0)-1/2|\ddot{a}_0|(u-u_0)^2$ locally, where $\ddot{a}_0<0$ is the second derivative of a suitably smoothed version of $A(u)$, evaluated at $u=u_0$. The critical trajectory is then found to have $\mathcal{R}-e=-\zeta(u-u_0)$, with $\zeta\equiv$ a positive constant [whence Eq. (A1) indeed holds]. Making this ansatz in Eq. (A4) determines ζ and leads to $A(u_0)=A_{crit}$, with

$$\frac{A_{crit}}{\sqrt{\tau}}-e^{-1}=\lambda e^{3/2}|\ddot{a}_0|^{1/2}\tau^{-5/4}\geqslant 0. \tag{A5}$$

The difficulty as to exploit Eq. (A5) is to evaluate $|\ddot{a}_0|$, and decide when it has to be selected.

A more refined analysis of Eq. (A4) proceeds by setting $\mathcal{R}-e=(2e^3\lambda/\tau)(d\psi/\psi du)$, which converts Eq. (A4) into the quantumlike problem:

$$\frac{2\Lambda^2}{\tau^2}\frac{d^2\psi}{du^2}+\psi\left[\left(\frac{A(u_0)}{\sqrt{\tau}}-\frac{1}{e}\right)-\left(\frac{A(u_0)-A(u)}{\sqrt{\tau}}\right)\right]=0, \tag{A6}$$

with $\Lambda=e^{3/2}\lambda$. The critical trajectory $\mathcal{R}-e$ (decreasing but not going to $-\infty$ in finite time) corresponds to the fundamental, hence nodeless [21], solution to Eq. (A6). In the parabolic approximation that led to Eq. (A5), $\psi^2\sim\exp(-\varpi^2(u-u_0)^2)$ and

$$\varpi^2=|\ddot{a}_0|^{1/2}\tau^{3/4}/2\Lambda. \tag{A7}$$

It thus transpires that a more accurate modeling should choose $|\ddot{a}_0|$ as some average of $\ddot{A}_0$ weighted by a function whose spread depends...on $|\ddot{a}_0|$ itself. The Rayleigh-Ritz [21] variational method to estimate the lowest ''energy-level'' $A(u_0)/\sqrt{\tau}-1/e$, employed here with $\psi^2\sim\exp(-\varpi^2(u-u_0)^2)$ as two-parameter trial function, confirms this viewpoint: it yields the two conditions

$$\int_{-\infty}^{+\infty}\frac{dA(u)}{du}\exp(-\varpi^2(u-u_0)^2)\varpi\frac{du}{\sqrt{\pi}}=0, \tag{A8}$$

$$\int_{-\infty}^{+\infty}\frac{d^2A(u)}{du^2}\exp(-\varpi^2(u-u_0)^2)\varpi\frac{du}{\sqrt{\pi}}=\ddot{a}_0, \tag{A9}$$

provided ϖ^2 is written as in Eq. (A7).

The allowed u_0 are maxima ($\ddot{a}_0\leqslant 0$) of $A(u)$, once the latter has been filtered by ψ^2; and Eq. (A9) identifies $\ddot{a}_0$ with the second derivative of the ϖ-filtered version, $a(u)$, of $A(u)$ at such points. Even once restricted by the constraints $\ddot{a}_0\leqslant 0$ and $A(u_0)\geqslant\sqrt{\tau}/e$ (this follows from the existence of a bound state) Eqs. (A8) and (A9) allow for infinitely many solutions $(u_0,\ddot{a}_0)$, in finite number per unit time.

Discarding all numerical factors (e.g., π, $4e^2$, Λ^2, ...), we next approximate $|\ddot{a}_0|\equiv(\ddot{a}_0^2)^{1/2}$ by $\langle\ddot{a}^2\rangle^{1/2}$, which is likely an upper bound because the constraint (A8) and any cancelation of small scale variations of $\ddot{A}$ are neglected. From the structure of Eq. (A9), we further relate $\langle\ddot{a}^2\rangle$ to the spectral power density $\mathcal{S}(\omega)$ of $A(u)$ by

$$\langle\ddot{a}^2\rangle\sim\int_0^{\varpi}\omega^4\mathcal{S}(\omega)d\omega, \tag{A10}$$

where the upper limit ϖ follows from the effective range of the Gaussian involved in Eq. (A9).

For very smooth $A(u)$'s [e.g., deduced from the χ_i's introduced in Sec. V C, that have $\mathcal{S}(\omega \gg 1) \sim \omega^{-6}$], the integral in Eq. (A10) converges whatever $\varpi \gg 1$. Since $\langle A^2 \rangle \sim \mu$ by Eq. (43), the estimate

$$\frac{A_{crit}}{\sqrt{\tau}} - e^{-1} \sim \mu^{1/4} \tau^{-5/4} \tag{A11}$$

follows from Eq. (A5), up to numerical constants.

For explicitly *and* μ-filtered $A(u)$'s, $\mathcal{S}(\omega) \sim \mu \omega^{-4}/(1+\omega^2/\mu^2)$ at frequencies $\omega \gg 1$, thereby producing a RHS of Eq. (A10) of order $\mu \min(\varpi, \mu)$; combining Eqs. (A5) and (A7) yields

$$\frac{A_{crit}}{\sqrt{\tau}} - e^{-1} \sim \begin{cases} \mu^{2/7} \tau^{-8/7}, \\ \mu^{1/2} \tau^{-5/4}, \end{cases} \tag{A12}$$

depending on whether $\mu^2 \gg \tau$ or $\mu^2 \ll \tau$, again up to pure numbers,

For stimuli that are not explicitly filtered [merely μ filtered; see Eq. (19)], and have $\mathcal{S}(\omega) \sim \mu \omega^{-2}/(1+\omega^2/\mu^2)$ as implied by Fig. 8 and Eq. (36), similar asymptotics yields $\langle \ddot{a}^2 \rangle \sim \mu \varpi \min(\varpi^2, \mu^2)$; then, through Eqs. (A5) and (A7), one gets

$$\frac{A_{crit}}{\sqrt{\tau}} - e^{-1} \sim \begin{cases} \mu^{2/5} \tau^{-4/5}, \\ \mu^{3/7} \tau^{-4/7}, \end{cases} \tag{A13}$$

depending on whether $O(\mu^4) >$ or $< O(\tau^3)$. As in Eqs. (A11) and (A12), the difficulties about comparing Eq. (A13) to numerics arise from the present neglect of all numerical constants (some of which may be $\gg 1$ or $\ll 1$), and from the restricted range of μ's and τ's that are accessible to extensive numerical solutions of Eq. (20).

APPENDIX B: JOINT STATISTICS OF TOTAL STRAIN AND ITS DERIVATIVE

Let $\mathbf{K} = (K_1, K_2, K_3)$ denote 3 independent, stationary and Gaussian random processes (e.g., the H_i's, the h_i's or the χ_i's) with a common rms value σ. The notation $\dot{\mathbf{K}}$ will stand for their u derivatives, assumed to have the same upper cutoff frequency Ω [e.g., $O(\mu)$ or $O(1)$]. Defining $\Upsilon \equiv (\Upsilon_1^2 + \Upsilon_2^2 + \Upsilon_3^2)^{1/2}$, with $\Upsilon_i = K_i - \Sigma_j^3 K_j/3$ in analogy with Eq. (18), we are here interested in the joint probability density $\Pi(\Upsilon, \dot{\Upsilon})$ of Υ and of $\dot{\Upsilon} \equiv d\Upsilon/du$.

By definition $\Pi(\Upsilon, \dot{\Upsilon}) d\Upsilon d\dot{\Upsilon}$ is the integral

$$\mathcal{M} = \int \frac{d\mathbf{K}}{(2\pi\sigma^2)^{3/2}} \frac{d\dot{\mathbf{K}}}{(2\pi\Omega)^{3/2}} \exp\left(- \frac{\mathbf{K}\cdot\mathbf{K}}{2\sigma^2} - \frac{\dot{\mathbf{K}}\cdot\dot{\mathbf{K}}}{2\Omega} \right) \tag{B1}$$

extended to the domain $\Upsilon \leqslant (\Upsilon_1^2 + \Upsilon_2^2 + \Upsilon_3^2)^{1/2} \leqslant \Upsilon + d\Upsilon$, $\dot{\Upsilon} \leqslant (\dot{\Upsilon}_1 \Upsilon_1 + \dot{\Upsilon}_2 \Upsilon_2 + \dot{\Upsilon}_3 \Upsilon_3)/\Upsilon \leqslant \dot{\Upsilon} + d\dot{\Upsilon}$.

To evaluate $\mathcal{M}$, we first set

$$\mathbf{K} = \mathbf{U}\mathbf{k}, \quad \dot{\mathbf{K}} = \mathbf{L}\dot{\mathbf{k}}, \tag{B2}$$

where the matrices $\mathbf{U}$ and $\mathbf{L}$ are orthogonal and such that $k_3\sqrt{3} = K_1 + K_2 + K_3$, $\dot{k}_3\sqrt{3} = \dot{K}_1 + \dot{K}_2 + \dot{K}_3$ [32]. This choice is motivated by the identify $\Upsilon^2 \equiv \Sigma_1^3 K_i^2 - 1/3(\Sigma_1^3 K_j)^2$ which is $\Upsilon^2 = k_1^2 + k_2^2$ in terms of the new variables. Equation (B1) becomes

$$\mathcal{M} = \int \frac{dk_1 dk_2}{2\pi\sigma^2} \frac{d\dot{k}_1 d\dot{k}_2}{2\pi\Omega} \exp\left(- \frac{k_1^2 + k_2^2}{2\sigma^2} - \frac{\dot{k}_1^2 + \dot{k}_2^2}{2\Omega} \right) \tag{B3}$$

after Gaussian integrations over k_3 and $\dot{k}_3$; the integration domain in Eq. (B3) is now $\Upsilon \leqslant (k_1^2 + k_2^2)^{1/2} \leqslant \Upsilon + d\Upsilon$, $\dot{\Upsilon} \leqslant (\dot{k}_1 k_1 + \dot{k}_2 k_2)/\Upsilon \leqslant \dot{\Upsilon} + d\dot{\Upsilon}$. Switching to the "polar" coordinates $(r, \theta, \dot{r}, \dot{\theta})$, with $k_1 = r\cos\theta$, $k_2 = r\sin\theta$, $\dot{k}_1 = \dot{r}\cos\theta - r\dot{\theta}\sin\theta$,... (the Jacobian of which change is r^2), finally yields $\Pi(\Upsilon, \dot{\Upsilon})$ in the form

$$\Pi(\Upsilon, \dot{\Upsilon}) = \frac{\Upsilon}{\sigma^2} \exp\left(- \frac{\Upsilon^2}{2\sigma^2} \right) \frac{\exp(-\dot{\Upsilon}^2/2\Omega)}{(2\pi\Omega)^{1/2}} \tag{B4}$$

after simple integrations over the angles $(\theta, \dot{\theta})$. Notice that $\Pi(\Upsilon, \dot{\Upsilon})$ is here proportional to $\int \Pi(\Upsilon, \dot{\Upsilon}) d\dot{\Upsilon} \equiv P_\Upsilon(\Upsilon)$.

APPENDIX C: PDF OF TOTAL STRAIN IN A NON-GAUSSIAN CASE

When the independent noises $\mathbf{K} = (K_1, K_2, K_3)$ follow Eq. (52), the PDF, $P_\Upsilon(\Upsilon)$ of the corresponding total strain results from the integral

$$\mathcal{V} = \int \prod_{i=1}^{3} \left(\exp\left(\frac{\pi}{2} K_i \right) + \exp\left(- \frac{\pi}{2} K_i \right) \right)^{-1} d\mathbf{K} \tag{C1}$$

over the domain $\Upsilon \leqslant (\Upsilon_1^2 + \Upsilon_2^2 + \Upsilon_3^2)^{1/2} \leqslant \Upsilon + d\Upsilon$, with Υ_i's defined in terms of the K_i's analogously to Eq. (18). We make a change of variables as in Eq. (B2), with a matrix $\mathbf{U}$ consisting of $(-1,2,1)/\sqrt{6}$, $(1,0,-1)/\sqrt{2}$ and $(1,1,1)/\sqrt{3}$ as mutually orthogonal, normed column vectors. An elementary integration over $X = \exp((\pi/2)(k_3/\sqrt{3}))$ converts $\mathcal{V}$ into an integral over (k_1, k_2), extended to the domain $\Upsilon \leqslant (k_1^2 + k_2^2)^{1/2} \leqslant \Upsilon + d\Upsilon$. Passing to polar coordinates ultimately produces $P_\Upsilon(\Upsilon)$ as

$$P_\Upsilon(\Upsilon) = \Upsilon \int_0^{2\pi} \frac{\sqrt{3}}{(X_1 + X_2)(X_2 + X_3)(X_3 + X_1)} d\theta, \tag{C2}$$

with $X_j = \exp((\pi\Upsilon/\sqrt{6})\cos(\theta - \theta_j))$ and $\theta_j = (-\pi/3, 0, \pi/3)$, whereby $X_1 X_2 X_3 \equiv 1$.

For $\Upsilon \to 0$, $P_\Upsilon(\Upsilon) \sim \Upsilon$. For $\Upsilon \to \infty$, the integrand in Eq.

(C2) quickly reduces to $\sim \min(X_j)/\max(X_j)$, except in $O(1/\Upsilon)$ neighborhoods of its maxima ($2\pi m/6$, $m=0...5$, mod 2π), where two X_j's cross and the integrand is locally rounded into sech$(\cdot)$ functions: $P_\Upsilon(\Upsilon\to\infty)\sim\exp(-(\sqrt{6}\pi/4)\Upsilon)$ results from integration of the latter.

Gaussian K_i's are atypical in the sense that in the analog of Eq. (C2) the integrand is independent of θ: the prefactor ($\equiv\Upsilon$) does not disappear from $P_\Upsilon(\Upsilon\to\infty)$ any longer.

[1] F. A. Williams, *Combustion Theory* (Benjamin-Cummings, Menlo Park, 1985).

[2] A. Liñan and F. A. Williams, *Fundamental Aspects of Combustion* (Engineering Sciences, Oxford, 1993), Vol. 34.

[3] Y. B. Zel'dovich, G. Barenblatt, V. Librovich, and G. Makhviladze, *The Mathematical Theory of Combustion and Explosions* (Consultant Bureau, New York, 1985).

[4] B. Deshaies and G. Joulin, Combust. Sci. Technol. **37**, 99 (1984).

[5] J. Buckmaster and G. Joulin, J. Fluid Mech. **227**, 407 (1991).

[6] J. D. Buckmaster, G. Joulin, and P. Ronney, Combust. Flame **79**, 381 (1990).

[7] J. D. Buckmaster, G. Joulin, and P. Ronney, Combust. Flame **84**, 411 (1991).

[8] O. C. Kwon *et al.*, Seventh International Workshop on Microgravity Combustion and Chemically Reacting Systems, Cleveland, OH, 2003 (unpublished).

[9] G. Joulin, Combust. Sci. Technol. **43**, 99 (1985).

[10] G. Joulin, P. Cambray, and N. Jaouen, Combust. Theory Modell. **6**, 53 (2002).

[11] H. Rouzaud, Ph.D. thesis, Université de Toulouse III, France, 2003.

[12] G. K. Batchelor, J. Fluid Mech. **95**, 369 (1979).

[13] G. Uhlenbeck and L. Ornstein, *Selected Papers on Noise and Stochastic Processes*, edited by N. Wax (Dover, New York, 1954), p. 93.

[14] P. N. Brown, G. D. Byrne, and A. C. Hindmarsh, SIAM (Soc. Ind. Appl. Math.) J. Sci. Stat. Comput. **10**, 1038 (1989).

[15] S. O. Rice, *Selected Papers on Noise and Stochastic Processes* (Ref. [13]), pp. 133–293, especially Eq. 3.3-2 therein.

[16] M. Kac, Bull. Am. Math. Soc. **49**, 314 (1943).

[17] M. Mehta, *Random Matrices* (Academic, New York, 1991).

[18] L. Landau and E. Lifshitz, *Fluid Mechanics* (Pergamon, Oxford, 1959).

[19] Y. D'Angelo and G. Joulin, Combust. Theory Modell. **5**, 1 (2001).

[20] R. Feynman and A. Hibbs, *Quantum Mechanics and Path Integrals* (McGraw-Hill, New York, 1965).

[21] P. Morse and H. Feshbach, *Methods of Theoretical Physics* (McGraw-Hill, New York, 1953), Vol. II.

[22] *Selected Papers on Noise and Stochastic Processes*, edited by N. Wax (Ref. [13]).

[23] S. Minaev, L. Kagan, G. Joulin, and G. Sivashinsky, Combust. Theory Modell. **5**, 609 (2001).

[24] That is to say, the FB is assumed not to propagate itself relative to the gas. A situation when this might occur is investigated in [23].

[25] The motive for this choice is threefold: the resulting processes are Gaussian, easy to generate and they (apparently) involve a single time scale t_{cor}.

[26] In the limit $\delta u\to 0^+$ and $u\gg 1$.

[27] Recall that the numerics actually employs $\tilde{A}(u)$, defined by $\tilde{A}(u\leqslant 0)=A(0)$ and $\tilde{A}(u\geqslant 0)=A(u)$.

[28] The seemingly arbitrary choice is motivated later; see Sec. VI.

[29] This ceases to be true when u_{life} becomes comparable to the actual duration of the extinction process, and is why Eq. (37) does not hold for $u_{life}\ll\langle u_{life}\rangle$; see Fig. 10.

[30] Thanks to the structure of Eq. (37), the probability that u_{life} would exceed some $u_{\max}$ is $\exp(-u_{\max}/\langle u_{life}\rangle)$; this could allow one to account for such long-lived flame-ball histories ($u_{life}\geqslant u_{\max}\gg 1$) in an iterative determination of $\langle u_{life}\rangle$ without actually computing $\mathcal{R}(u)$ beyond $u=u_{\max}$, thereby reducing the computational burden. Unfortunately, this significantly increases the uncertainty on the estimated $\langle u_{life}\rangle$.

[31] The H_i's are independent and Gaussian; having more than one large $|\mu H_i|$ at any one time is less frequent.

[32] Such matrices exist (see Appendix C).